

# The RFOFO Ionization Cooling Ring

R.B. Palmer<sup>1</sup>, V. Balbekov<sup>2</sup>, J.S. Berg<sup>1</sup>, S. Bracker<sup>3</sup>, L. Cremaldi<sup>3</sup>, R.C. Fernow<sup>1</sup>,  
J.C. Gallardo<sup>1</sup>, R. Godang<sup>3</sup>, G. Hanson<sup>4</sup>, and A. Klier<sup>4</sup>, and D. Summers<sup>3</sup>

<sup>1</sup>*Physics Department, Brookhaven National Laboratory, Upton, NY 11973*

<sup>2</sup>*Fermi National Accelerator Laboratory, Batavia, IL 60510*

<sup>3</sup>*University of Mississippi, Oxford, MS 38677*

<sup>4</sup>*University of California, Riverside, CA 92521*

(14 March 2005)

**Abstract.** Practical ionization cooling rings could lead to lower cost or improved performance in neutrino factory or muon collider designs. The ring modeled here uses realistic 3-dimensional fields. The performance of the ring compares favorably with the linear cooling channel used in the second US Neutrino Factory Study. The normalized 6D emittance of an ideal ring is decreased by a factor of  $\sim 240$ , compared with a factor of only 15 for the linear channel. We also examine such “real-world” effects as windows on the absorbers and rf cavities and leaving empty lattice cells for injection and extraction. For realistic conditions the ring increases the density of muons in a fixed acceptance volume by a factor of 4.2.

## I. INTRODUCTION

Designs for neutrino factories [1] and muon colliders [2] use ionization cooling to reduce the emittance of the muon beam prior to acceleration. Ionization cooling is currently the only feasible option for cooling the beam within the muon lifetime ( $\tau_0 = 2.19 \mu\text{s}$ ). If muons alternately pass through a material absorber, and are then reaccelerated, and if there is sufficient focusing at the absorber, then the transverse phase space is reduced, i.e. the muons are cooled in the transverse dimension. A consequence of the transverse cooling is an increase of the longitudinal phase space caused by energy straggling in the material. The momentum spread can be reduced if dispersion is introduced and a wedge-shaped absorber is placed such that high momentum particles pass through more material than low momentum particles. However, when this procedure is carried out the beam width is increased. The process is thus primarily an exchange of emittance between the longitudinal and transverse dimensions, but when combined with transverse cooling in the material, all three dimensions can be cooled.

Early muon collider studies had assumed that transverse cooling and emittance exchange would be done in alternating stages. The transverse cooling used straight channels with rf and absorbers, while the emittance exchange employed bent solenoids and wedges. A serious problem with this approach was found to be the matching that was necessary between the two types of lattices. However, there has been considerable progress over the past few years in achieving 6-dimensional ionization cooling in cooling rings [3]. Ring coolers can overcome much of this matching problem by

rapidly alternating the two functions. The first ring cooler design [4] was based on solenoid focusing. Alternate cells contained 1) transverse cooling in a long solenoid containing acceleration and a single hydrogen absorber; and 2) emittance exchange in a cell containing two bend magnets, two opposed solenoids, and a LiH wedge. Matching between them has currently been achieved only with hard-edged magnetic fields. Each pair of cells is long enough that at least one half integer betatron resonance is present within the momentum acceptance. Later quadrupole-focused rings [5] took the process a step further, using a single cell type in which a wedge absorber cooled in both longitudinal and transverse phase space. These ideas eased the lattice design, but introduced some transverse emittance growth from energy straggling in the absorber, since it was now in a dispersive location. In addition, the weaker focusing in such quadrupole lattices limit the available amount of cooling and momentum acceptance. Current versions of this ring design use edge-focused dipoles instead of quadrupoles and high pressure gas instead of wedge absorbers.

At present the most realistic modeling has been done for the RFOFO cooling ring [6-9]. The ring discussed here follows the quadrupole design in employing a single cell for doing both transverse cooling and emittance exchange. However, we use solenoidal focusing to obtain larger angular and momentum acceptances. The cell includes dispersion, acceleration, and energy loss in a single thick hydrogen wedge. The FOFO part of the name refers to the focusing-drift-focusing nature of the solenoid lattice, in analogy to the FODO lattice for quadrupole channels. The prefix **R** designates a particular type of FOFO lattice where the magnetic cell has the same length as the geometric cell. As a result the axial field changes polarity in the middle of the cell. The overall layout of the ring is shown in Fig. 1.

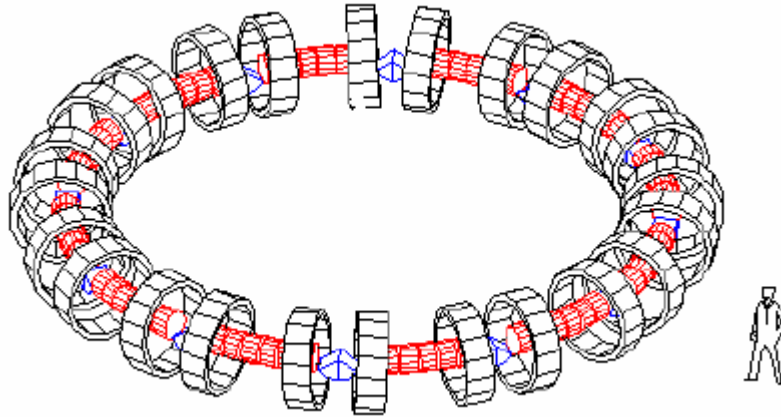


**Figure 1.** Layout of the RFOFO cooling ring [10]. The large black cylinders are solenoids, the small red cylinders are rf cavities, and the blue wedges are hydrogen absorbers.

Two solenoids in each cell with opposite polarity provide transverse focusing. The solenoids are not equally spaced; those on either side of the absorbers are closer together in order to increase the focusing at the absorber. The bending field is provided by alternately tipping the axis of the solenoids above and below the orbital

midplane. The bending also provides the dispersion necessary for emittance exchange. A short cell length is used to obtain a small beta function with a reasonable value of the solenoid field strength. Wedge-shaped absorbers are placed in the beam path at locations where the solenoidal field changes direction. Most of the lattice cell is filled by rf cavities to restore the energy lost in the absorbers. The lattice has dispersion at the rf cavities, which introduces synchro-betatron mixing. Performing the transverse cooling with an absorber where there is dispersion also introduces additional emittance growth. However, we find that these disadvantages are compensated by the greater acceptance from the use of a single repeating cell with no integer or half-integer betatron resonances in the momentum acceptance. In addition the longitudinal cooling provided by the wedge-shaped absorber minimizes losses from particles falling out of the rf bucket

## II. MODELING THE RING

A more detailed layout of three cells of the ring is shown in Fig. 2 and a summary of ring properties are given in Table 1.

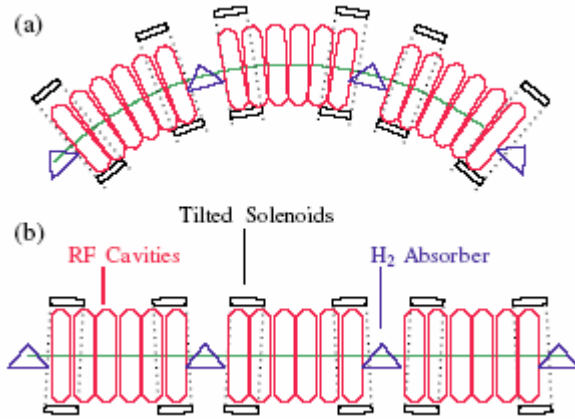


**Figure 2.** Three cells of the RFOFO lattice; (a) plan, (b) side view.

The 33 m circumference ring is made up of 12 identical, 2.75 m long cells. The magnetic field is produced by 50 cm long solenoids with an inner radius of 77 cm and an outer radius of 88 cm. The current density is  $\pm 95.27$  A/mm<sup>2</sup>. The longitudinal field on-axis has an approximately sinusoidal dependence on position. The tip angle of the solenoids was adjusted to provide a mean vertical bending field of 0.125 T. No attempt was made to set the field index  $n$  to a value of 0.5, so the focusing is different in  $x$  and  $y$ . However, the solenoids effectively mix  $x$  and  $y$ , so this is not a concern. The centers of the solenoids are displaced radially outwards from the 33 m reference circle by 10 cm to minimize the integrated amount of on-axis radial field, which causes vertical beam deviations.

**Table 1.** RFOFO ring parameters.

circumference	33	m
cells	12	
max. axial field	2.77	T
coil tilt angle	3	degrees
avg. vertical field	0.125	T
avg. momentum	220	MeV/c
min. transverse beta function	38	cm
max. dispersion function	8	cm
wedge opening angle	100	degrees
wedge thickness on-axis	28	cm
rf frequency	201.25	MHz
peak rf gradient	12	MV/m
rf phase from 0-crossing	25	degrees

The RFOFO ring was modeled using three independent simulation codes. One code was specifically written to examine this problem [11-12]. The second code was ICOOL [13], which has been widely used for neutrino factory and muon collider simulations. It includes a flexible system for specifying the problem geometry and magnetic fields. For the application here fields were either read in from an external file or calculated from on-axis multipoles. RF cavities were modeled as pillboxes, including the Bessel function radial dependence. Many of the energy loss, scattering and straggling routines in ICOOL are based on GEANT 3.21 [14]. The third code was the simulation software, MUC\_GEANT [15], which is an application of GEANT 3.21, specially designed for muon cooling simulations. The Runge-Kutta routine was changed to include electric fields, so that rf acceleration would be simulated properly. The software is also data-driven, i.e. it allows the user to change the cooling channel parameters, such as geometry, rf frequency/gradient and physics processes, without changing the code. The magnetic field was read in from an external file. The rf was modeled as a purely axial field with no transverse variation.

The 3-dimensional magnetic field from the ring of tipped solenoids was calculated in three other independent codes by summing the fields from a system of current sheets [12,16,17]. There are some complexities in generating the fields for small rings which are much less important for straight cooling channels. The coils being used in this design are large-diameter, short, and carry high-current; the maximum field is several tesla. The ring is small, a little over 5 meters in radius. We ignore for the moment the presence of any shielding iron. Then from every point in the active (muon-accessible) region of the ring, a particle is significantly affected by the field generated by all the coils, even the ones on the other side of the ring. Hence one must develop a single global field map, rather than assuming that a particle sees field components only from the closest coils. The field of a solenoidal current sheet can be written analytically in terms of elliptic integrals. The fields could also be generated from a set of coils using the Biot-Savart law. The resultant field components between the two methods agreed

well and were shown to satisfy Maxwell's equations to a high level of accuracy. Because the fields were modeled from coils, all magnetic end field effects are automatically included in the simulations. The on-axis field components for one cell are shown in Fig. 3.

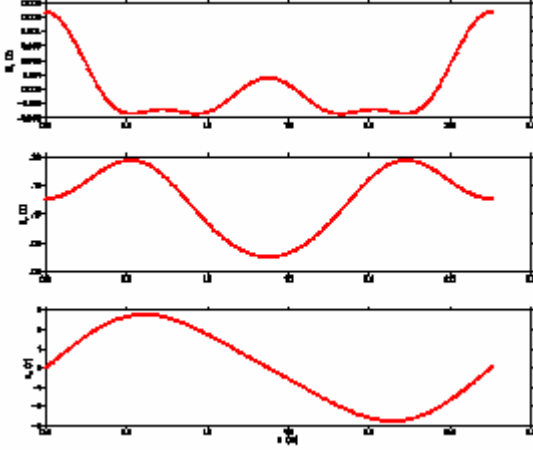


**Figure 3.** Magnetic field on-axis for one cell. The upper panel is  $B_x$ , the middle panel is  $B_y$  and the lower panel is  $B_s$ .

Once the magnetic field generator was working subsequent tracking could be done from the field calculated on a grid and saved to a map or from multipoles [18] of the field calculated around a reference circle. Figure 4 shows the calculated multipoles for one cell of the ring.

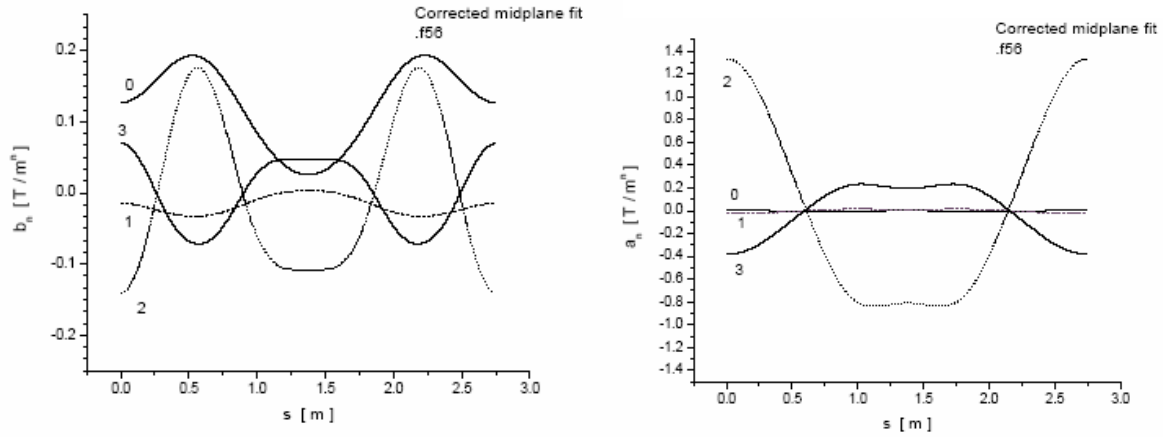


**Figure 4.** On-axis normal (left) and skew (right) multipoles in one cell of the RFOFO ring.

The on-axis transverse field has a rich spectrum of higher normal and skew multipoles.

Each lattice cell contains 6 rf cavity cells, each 33 cm long. The transit time factor for the cavity cells is 0.901. In ICOOL the rf cavities were modeled using cylindrical pillboxes running in the TM010 mode. The frequency is 201 MHz and the peak accelerating gradient is 12 MV/m. The cavity operates at a synchronous phase  $25^\circ$  off the 0-crossing point. The cavities are located in a dipole field in this design. Since we are accelerating muons, the cavities can be enclosed with metallic end windows in order to produce the maximum electric field on-axis for a given amount of rf power (maximum shunt impedance). The rf windows were stepped in thickness radially, in order to provide minimum thickness near the beam axis and still control the temperature increase due to rf heating.

The liquid hydrogen wedge absorbers have a “house” shape, as shown in Fig. 5, and are located in dispersive regions in order to decrease the momentum spread in the beam.

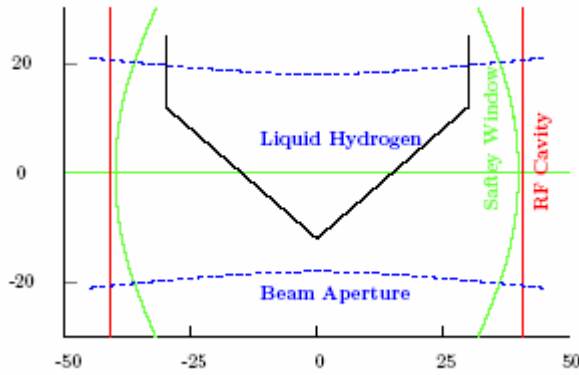


**Figure 5.** Wedge absorber used in some of the simulations.

The wedge only extends part way across the gap, such that a particle on the reference orbit always loses the same amount of energy crossing the wedge. The mean energy loss per cell was 8.4 MeV. The simulated absorber windows were planar and located axially just in front of and behind the wedge itself. In reality the window shape will conform to the shape of the absorber and the effect on the beam of scattering in the window should be lessened. Because of the small bending field we use a wedge with maximum possible opening angle, which has zero thickness on one side. This combination of dispersion and wedge provides adequate emittance exchange between the transverse and longitudinal phase spaces. The wedge has a central thickness of 28 cm, a total wedge opening angle of  $100^\circ$  and is rotated  $30^\circ$  from the vertical.

### III. LATTICE FUNCTIONS AND BEAM DYNAMICS

For our initial studies of the basic lattice functions and beam dynamics we consider the ring with the magnetic field present, but no rf or absorbers. This enables us to simply study some of the basic features of the lattice, such as acceptances, beta function, closed orbits and dispersion functions.

## A. Acceptance

We first examine the acceptance of the magnetic lattice as a function of momentum. A series of particles with small deviations from the closed orbit were tracked through one cell of the ring lattice. The eigenvalues were then extracted from the resulting linear transport matrix. The magnitude and phase of the largest eigenvalue are shown in Fig. 6.

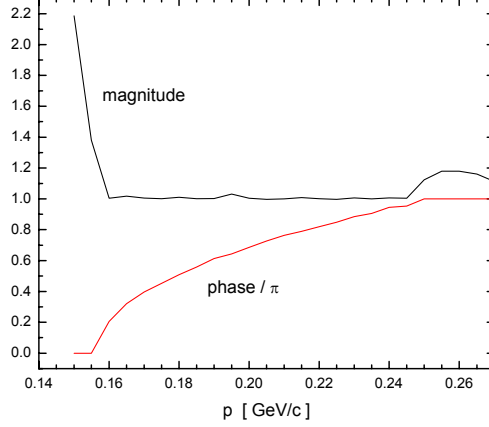


**Figure 6.** Magnitude and phase of the largest eigenvalue for the one-cell transport matrix

The magnitude is very close to 1 over the momentum band from 160 to 245 MeV/c. The ring has a very weak linear difference coupling resonance excited by the bend of the channel [11]. In practice this resonance is suppressed by the cooling.

In Fig. 7 we examine the dynamic acceptance of the lattice, with no rf or absorber, for three different bending fields: 0.0 T, 0.125 T, and 0.25 T. Using ICOOL, particles are injected into the lattice at 9 different momenta and 6 different angles. In the plots particles that were lost are marked by dots, and those that survive up to 275 m are plotted as circles.

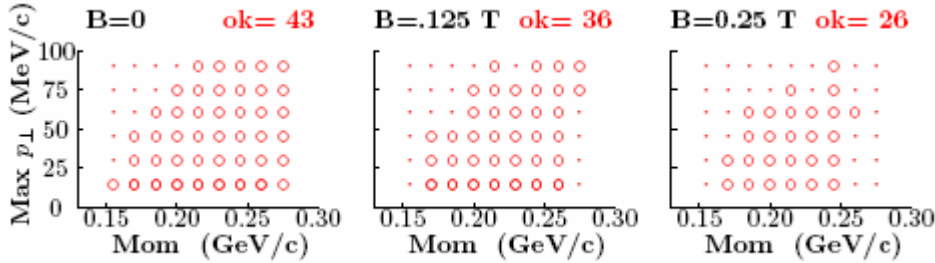


**Figure 7.** Ring acceptance for varying vertical field.

Out of a maximum of 54 particles, the numbers transmitted for the three fields (0, .125, and .25 T) are 43, 36, and 26. Clearly, the acceptance is reduced

as the bending field is increased. We may thus expect that it is best to use the least bending field consistent with adequate emittance exchange.

## B. Beta function

Figure 8(a) shows the beta function as a function of position along a cell. The minimum value of the beta function at the center of the absorber and at the central momentum is about 38 cm.

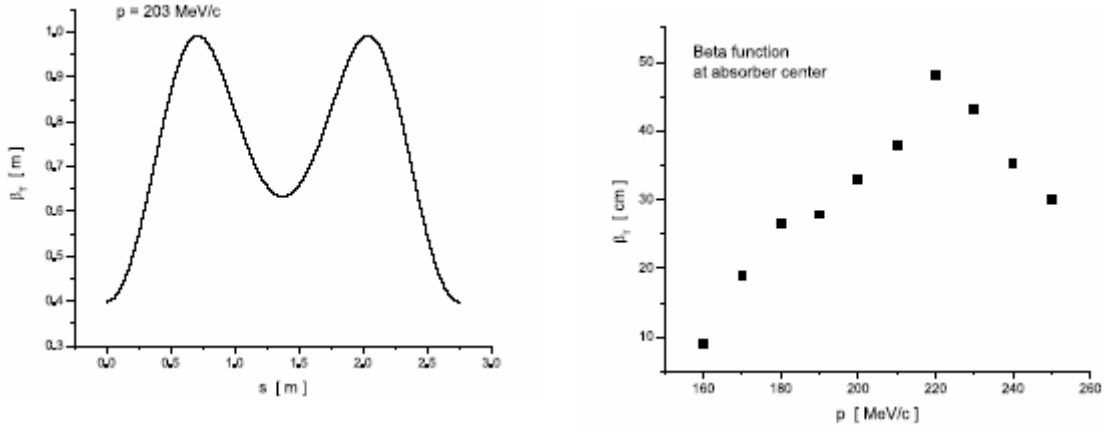


**Figure 8.** (a) Beta function vs. position in the cell; (b) beta function vs. muon momentum.

Figure 8(b) shows the beta function as a function of the muon beam momentum. This also shows that the lattice transmits particles in the momentum band 160 - 250 MeV/c. These limits are determined by very strong  $\pi$  and  $2\pi$  resonances at the limiting momenta.

## C. Closed orbits

Because of the symmetry of the magnetic field, radial and vertical deviations of the closed orbit must be even functions of  $s$  at any energy. This requires that their derivatives must be 0 at the ends of the period. This makes it easier to search for closed orbits because only variations in  $x_0$  and  $y_0$  need be considered. Muons were “injected” at the boundary of the cell, in the middle of the absorber, which is one of the two planes in a cell where the transverse momentum vanishes for a closed orbit. For each initial (longitudinal) momentum, a unique closed orbit was determined by scanning the plane, and finding the point to which the muon returns every time it crosses the measuring plane at the middle of the absorber.



Since the magnetic field has a small radial component on-axis, the closed orbits are non-planar. Figure 9 shows the transverse motion of the closed orbit for a 200 MeV/c muon.

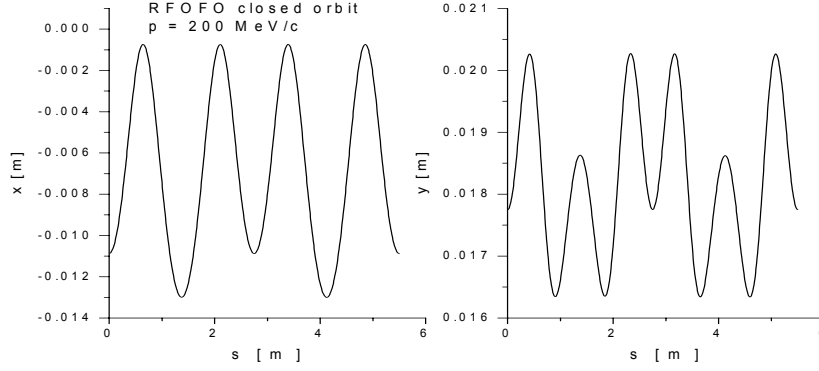


**Figure 9.** Transverse position of a closed orbit along two cells of the system axis.  $y$ : vertical,  $x$ : radial position.

Note that the closed orbit is offset by 11 mm in  $x$  and by 18 mm in  $y$  at the beginning of the cell. Along the cell  $x$  varies by  $\pm 6$  mm and  $y$  varies by  $\pm 2$  mm. Some of the closed orbits are shown as a function of momentum in Fig. 10.

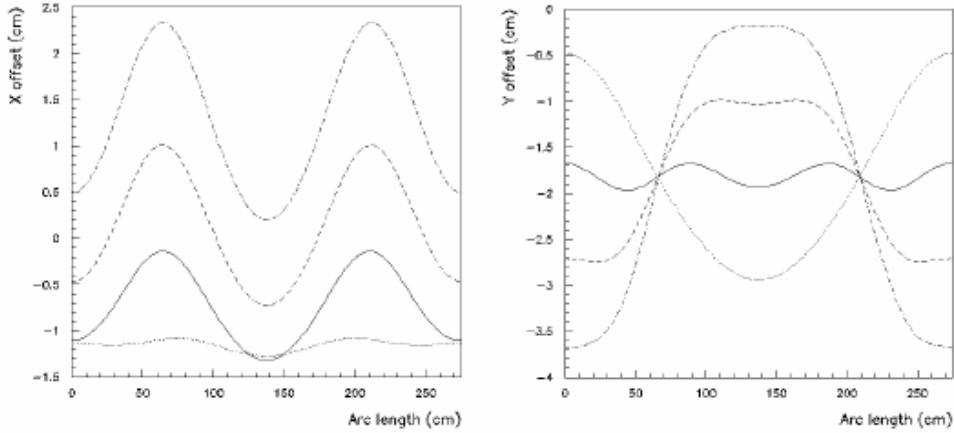


**Figure 10.** Closed orbits as a function of momentum.

#### D. Dispersion function

Dispersion functions in  $x$  and  $y$  at the absorber central plane (and approximately the absorber as a whole) can be derived from the closed orbits. One can see the linear dependence of the  $y$  (vertical) offset on the energy in Fig. 11. The dispersion at the absorber is approximately 8 cm in a direction  $30^\circ$  from the  $y$  axis.

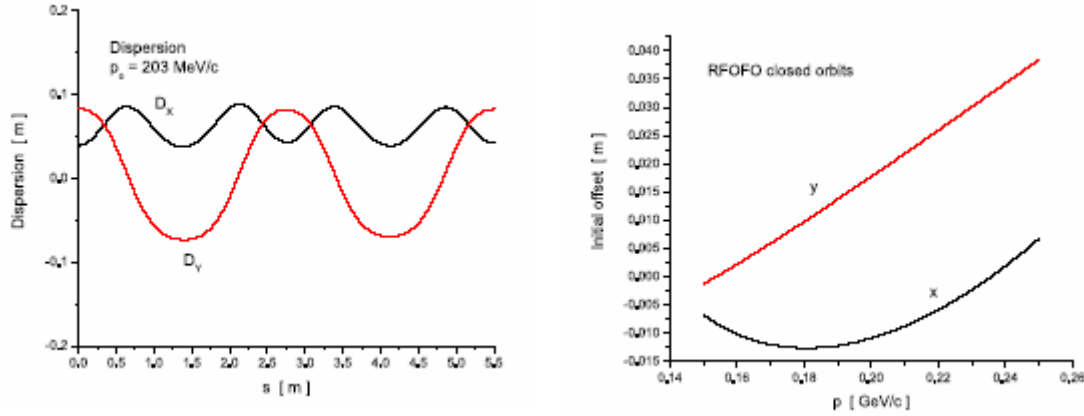


**Figure 11.** (left) Dispersion vs. position in the cell; (right) dispersion vs. muon momentum.

The dispersion at the center of the rf cavity has the opposite sign, and is also mostly in the y direction. The vertical dispersion is surprisingly linear as a function of momentum, but the radial dispersion is very nonlinear.

#### IV. COOLING SIMULATIONS: IDEAL RING

We now turn to simulations of muon beams in the ring. For cooling studies we must now include the rf cavities and absorbers in the simulations.

Several merit factors have been defined for quantifying cooling performance.

$$M(s) = \frac{\varepsilon_{6N}(initial)}{\varepsilon_{6N}(s)} Tr$$

$$D(s) = \frac{n(s)/V}{n(0)/V}$$

$$Q(s) = \frac{\frac{d\varepsilon_{6N}}{ds} \frac{1}{\varepsilon_{6N}}}{\frac{dN}{ds} \frac{1}{N}}$$

For the M-factor  $\varepsilon_{6N}$  is the normalized 6D emittance and Tr is the total muon transmission. For the D-factor, V is a fixed transverse and longitudinal phase space acceptance and  $n$  is the number of muons that are contained in V. The M-factor is more relevant for a muon collider, while the D-factor would be more applicable to a neutrino factory. The Q-factor is a local variable where N is the number of muons at location  $s$  [23].

We first examine the performance of an “ideal” ring, ignoring for the moment additional effects due to windows on the absorbers and rf cavities and leaving empty space for injection. Several important ring parameters are listed in Table 2.

**Table 2.** Ring parameters

$\rho$	5.252	m
$\alpha_p$	$1.52 \cdot 10^{-2}$	
$\gamma_T$	8.09	
$\eta$	-0.198	
$\beta_s$	6.06	m

The first quantity  $\rho$  is the mean radius of curvature. The momentum compaction  $\alpha_p$  is the fractional change in circumference per fractional change in momentum,  $\gamma_T$  is the transition energy factor, and  $\eta$  is the slip factor. This ring always operates below the transition energy. The longitudinal beta function  $\beta_s$  is given by [24]

$$\beta_s^2 = \frac{-c\eta CE}{2\pi\beta f eV \cos\phi_s}$$

where  $C$  is the circumference of the ring,  $E$  is the energy of the muons,  $\beta$  is the relativistic velocity,  $e$  is the unit of charge,  $V$  is the peak rf voltage and  $\phi_s$  is the synchronous phase. Note that  $\beta_s$  is much larger than the transverse beta function  $\beta_T$ .

A reference particle was used to determine each cavity’s relative phase. The reference particle is a muon that runs in a closed orbit and is used as a “clock” to determine the rf frequency and set the entry times for each cavity in the ring. The clock should satisfy the following conditions:

- the revolution period must be an integer multiple of the rf pperiod
- the muon momentum should be around 200 MeV/c.

In GEANT the closed-orbit muon that was chosen as the reference particle has a momentum of 200.96 MeV/c. With a revolution period of 124.22 ns, its 25<sup>th</sup> harmonic is 201.26 MHz.

Figure 12 shows the performance of the ideal ring as a function of distance. The input beam for this simulation corresponds to the beam at the entrance to the linear cooling channel in the recent neutrino factory feasibility study (FS2) [20].

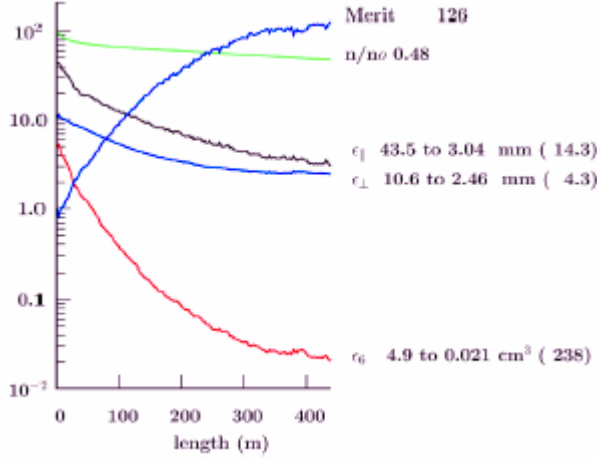


**Figure 12.** Transmission, normalized transverse, longitudinal and 6D emittances and merit factor M.

A separate analysis that decoupled the emittance planes gave normalized emittances  $\epsilon_{XN}=2.32$  mm,  $\epsilon_{YN}=1.81$  mm, and  $\epsilon_{ZN}=2.89$  mm. After a distance of 400 m ( $\sim 12$  turns) the 6D emittance has fallen by a factor of  $\sim 240$  with a transmission of 53% (66% without muon decay). The M-factor is 126. The same factor for the FS2 cooling lattice without windows is 15. The initial drop in transmission over the first few turns includes a contribution from scraping at transverse apertures due to mismatches between the initial beam distributions and the ring acceptance. This ideal ring has a D-factor of 8.6 and a Q-factor of 8.7.

We next show the idealized ring behavior in terms of the muon density. Figure 13 shows the total muon transmission together with the muon density into two fixed acceptance volumes. These volumes could correspond to the acceptance of a linear accelerator that follows the cooling ring at a neutrino factory.

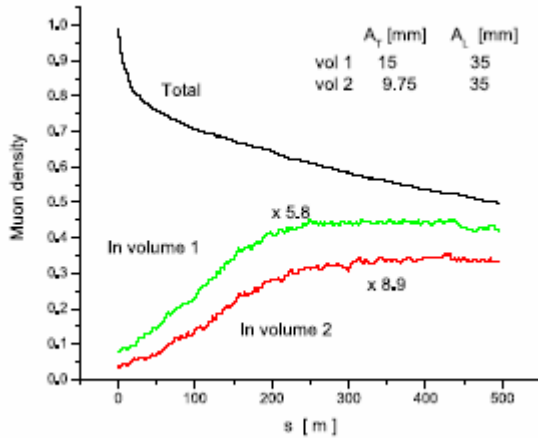


**Figure 13.** Performance of RFOFO ring. Transmission and muon density into two fixed acceptance volumes. These results were obtained using a  $100^\circ$  wedge.

The idealized ring increases the muon density into the smaller acceptance volume by a factor of almost 9 in 250 m, which corresponds to about 8 turns. The density in the larger acceptance volume increases by about a factor of 6.

For the remaining simulations we use a Gaussian input beam with normalized transverse emittance of 12 mm and normalized longitudinal emittance of 18 mm. For the ICOOL runs we used a circular reference particle with momentum of 203 MeV/c. This value was chosen to make the circulation time around the ring on a closed orbit equal to the 25th harmonic of 201.25 MHz. The initial beam had a correlation between the axial momentum and the transverse amplitude to minimize the tendency for the particles in the bunch to spread out longitudinally in the solenoidal field. The correlation causes the average axial momentum to be larger than the reference momentum of 203 MeV/c.

Figure 14 shows the radial and longitudinal phase space after 1 and 15 turns.

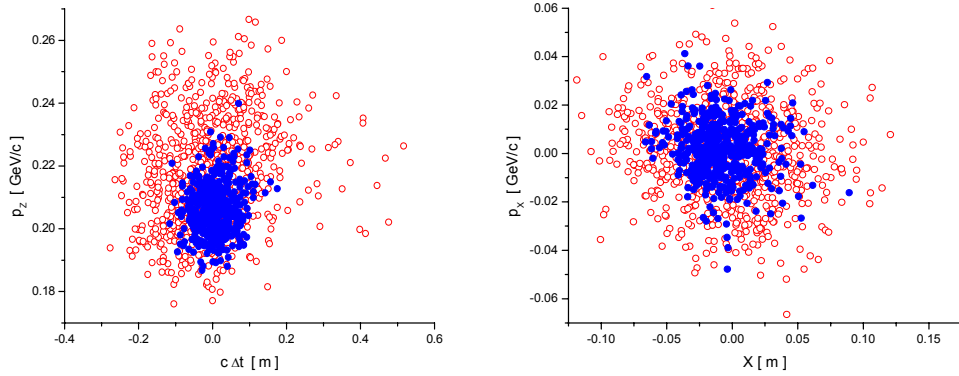


**Figure 14.** Longitudinal phase space (left) and radial phase space (right) after 1 turn (open circles) and 15 turns (closed circles).

The reduction of phase space area can be seen clearly in both distributions. The vertical transverse distribution is similar to the radial one because of the mixing caused by the solenoids.

A comparison of ICOOL and GEANT performance calculations are shown in Fig. 15. The emittance was calculated using the program ECALC9 [21], which is a standard tool used for this purpose.

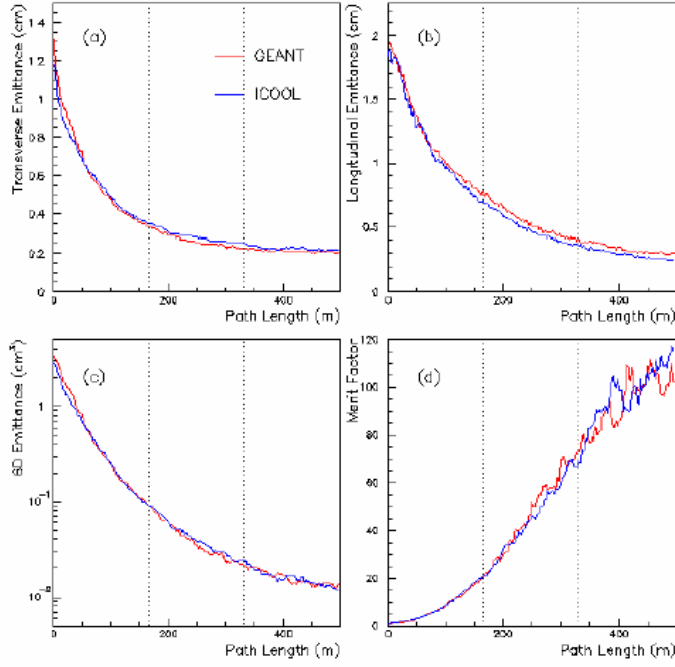


**Figure 15.** A comparison between GEANT (red line) and ICOOL (blue) for transverse emittance (a), longitudinal emittance (b), 6-dimensional emittance (c) and M-factor (d) in 15 ring turns. The dotted lines mark 5 and 10 turns.

The agreement in calculated performance between the two codes is excellent.

## V. COOLING SIMULATIONS: REALISTIC RING

We now consider the effects on performance of including windows for the absorbers and rf cavities and leaving empty cells for injection. We refer to this as the “realistic” ring design. The introduction of windows introduces new sources of scattering and degrades the cooling performance. We enclose the liquid hydrogen absorbers with aluminum windows. The rf cavities have tapered beryllium windows. In general the M-factor is more sensitive to the presence of windows and requires more turns to reach a maximum than the D-factor. Two adjacent cells have the absorber and rf cavities removed in order to leave space for the injection kicker, but the magnetic periodicity is maintained.

Table 3 shows the results of including these effects in the simulations.

**Table 3.** Perturbations on the ideal ring performance. FS2 stands for windows used in Study-2; FS2/20 stands for windows used in Study-2 with thicknesses reduced by a factor of 20.

absorber	abs window	rf window	empty cells	D-factor
LH	none	none	0	8.93
LH	250 $\mu\text{m}$ Al	none	0	7.50
LH	360 $\mu\text{m}$ Al	none	0	6.60
LH	500 $\mu\text{m}$ Al	none	0	6.08
LiH	none	none	0	4.88
LH	none	FS2	0	5.88
LH	none	FS2 / 20	0	7.80
LH	none	none	2	6.73
LH	360 $\mu\text{m}$ Al	FS2 / 20	2	4.25

The absorber window used in FS2 was 360  $\mu\text{m}$  of aluminum. We see that windows of this thickness degrade the performance by about 30%. For safety reasons it may be necessary to use an additional window that increases the total amount of aluminum. On the other hand the use of other special materials or optimized window shapes could reduce the amount of material required. Another possibility would be to replace the liquid  $\text{H}_2$  absorber with a solid material. LiH is one possible candidate, although Table 3 shows there is a 45% loss of performance with this option.

In FS2 the Be end windows on the rf cavities were 200  $\mu\text{m}$  thick from the axis out to a radius of 12 cm, then 400  $\mu\text{m}$  thick out to 18 cm. The interior windows were 700  $\mu\text{m}$  thick from the axis to a radius of 14 cm, then 1400  $\mu\text{m}$  thick out to 21 cm. These rf windows degrade the performance by about 35%. One possibility to get around this problem is to operate the cavities at liquid nitrogen temperature. The lower operating temperature and the reduced rf gradient of 12 MV/m versus 16 MV/m in FS2 allow the thickness of the windows to be decreased by a factor of 20 and the performance loss is only 13%. Alternatively, one could eliminate the rf cavity windows altogether and use an open cavity. This has the disadvantage that four times more power is required to produce the same  $E_z$  on axis.

Introducing two empty cells for injection/extraction reduces the performance by 25%. Finally, we consider an example that combines all of these effects. We choose liquid  $\text{H}_2$  as the absorber with FS2-like windows, assuming we can use this effective amount of aluminum because of improved alloys or window shape. We assume operation at liquid nitrogen temperature and use the thinner Be rf windows and leave the empty cells in the lattice for injection/extraction. Figure 16 shows the evolution of the D-factor for the realistic ring.

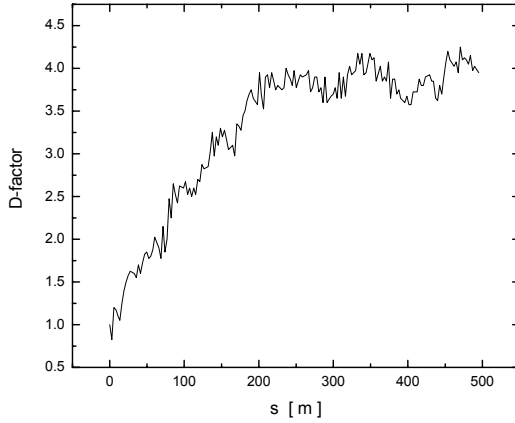


**Figure 16.** D-factor vs. distance for the realistic ring.

The phase space volume used in this simulation had a normalized transverse acceptance of 9.75 mm and a normalized longitudinal acceptance of 35 mm. The muon density into the accelerator acceptance peaks after about 8 turns. This realistic ring model still gives an impressive increase in the muon density of a factor of 4.25.

Figure 17 shows the evolution of the emittances and transmission for the realistic ring design.

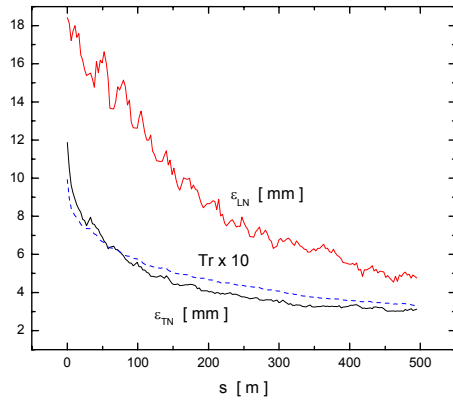


**Figure 17.** Normalized emittances and transmission with decay as a function of accumulated distance in the realistic cooling ring. One turn is 33 m.

Some of the transverse losses originate from particles that initially slip out of the rf bucket. Following this there is a steady loss due to decays. Initially the  $x$  emittance falls more rapidly than the  $y$  because it is the  $y$  emittance that is exchanged with the longitudinal. But the Larmor rotations in the solenoids soon mix the  $x$  and  $y$  emittances, bringing them to a common value. The emittance performance of the realistic ring is summarized in Table 4.



**Table 4.** Emittance performance of the realistic RFOFO cooling ring.

	initial	final	
$\epsilon_{TN}$	11.9	3.1	mm
$\epsilon_{LN}$	18.4	4.8	mm
$\epsilon_{6N}$	2830	51	mm <sup>3</sup>
Tr		33	%
M		19	

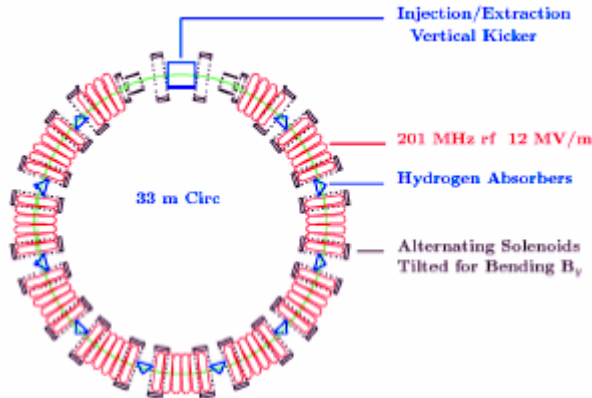
The mean angle of muons at the end of the channel was 66 mr and the maximum angle for an accepted particle was 200 mr. This illustrates the advantage of using solenoidal focusing for this application. Although the realistic ring merit factors are reduced considerably from the ideal ring, where the corresponding merit factors were  $M=112$  and  $D=8.9$ , the cooling performance is still quite significant.

## VI. DESIGN ISSUES

There are a number of difficult design issues that must be resolved before a real ring cooler can be designed. Each of the following areas needs a program of experimental R&D.

### A. Beam injection and extraction

The design of the injection/extraction channels and kickers will be challenging. The 12 fold symmetry of the ring must be broken to allow space for injection and extraction. In some simulations two cells have been modified for this purpose, as shown in Fig. 18.

**Figure 18.** Layout of RFOFO ring with injection/extraction cells.

A more detailed layout of the injection area is shown in Fig. 19.

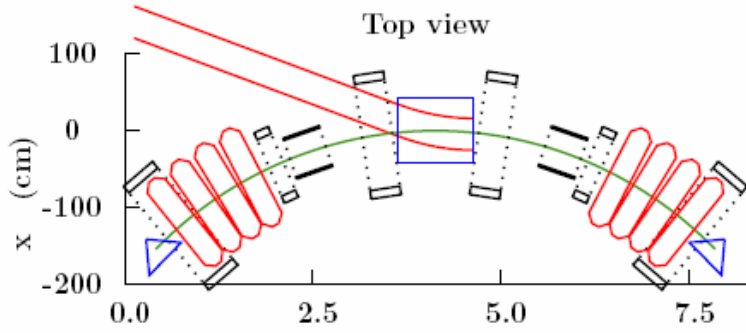


**Figure 19.** Injection/extraction area of the RFOFO ring.

The coils in the insertion area have been modified to allow muons from an external beamline to have access to the kicker. It is possible to generate magnetic fields in the insertion cells that are nearly identical to those in the rest of the ring.

The minimum pulsed energy required for the kicker is proportional to the square of the transverse emittance being kicked. Since the initial muon emittances discussed here are much larger than those encountered in other applications, such as antiproton accumulation, the energy in the pulsed kicker is three orders of magnitude greater, e.g.  $\sim 10000$  J compared with 10-20 J. However, magnetic amplifiers used in induction accelerators can provide this kind of pulse energy at the required pulse lengths, and a kicker design based on this concept has been proposed [22].

## B. Absorber heating

Using a ring for ionization cooling causes the beam bunches to pass through a given absorber many times. This results in the thermal load on the absorber in a ring being much larger than for the same absorber used in a linear channel. Consider the example shown in Table 5, which uses a 1 MW beam with similar parameters to FS2.

**Table 5.** Absorber heating for FS2 example

muons/bunch	$4.6 \cdot 10^{12}$	
bunch rep rate	15	Hz
absorber length	28.6	cm
turns in ring	8	
energy deposit/bunch	94	J
avg beam radius	4	cm
temperature rise/bunch	0.21	oC
avg power dissipated	1.42	kW
flow for $\Delta T=2\text{oC}$	1.45	l/s
velocity in 5 cm pipe	0.74	m/s

The average power deposited in the absorber exceeds 1.4 kW.

### C. RF windows

We have seen that the M-factor is very sensitive to the window thicknesses used in the simulations. Figure 20 shows how the merit factor depends on the rf window thickness.

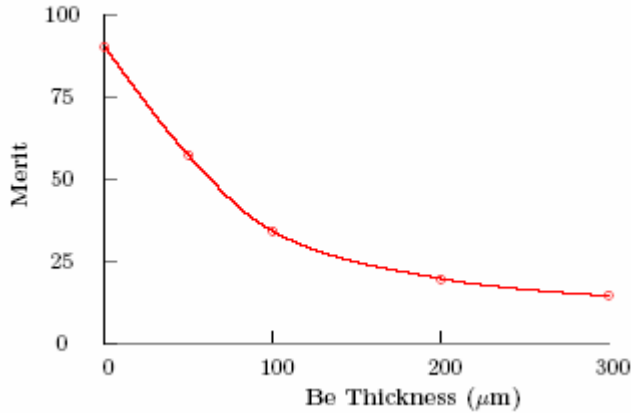


**Figure 20.** Dependence of M-factor on rf window thickness.

Thin windows are clearly advantageous and we would like to use beryllium window thicknesses on the order of 25  $\mu\text{m}$  if possible. Cooling the cavity to liquid nitrogen temperatures would help.

## VII. DESIGN VARIATIONS

We have also considered several variations of the 33 m circumference, 200 MHz ring discussed above.

### A. 16.5 m circumference ring

We have simulated [6] a case with twice the bending field (0.25 T) and thus a ring circumference of only 16.5 m. Such a ring would require an even shorter initial bunch train, and is not expected to have as good a dynamic aperture. The transmission of an ideal ring after 15 turns was 45%, the transverse normalized emittance was reduced from 10.8 to 3.6 mm, the longitudinal normalized emittance was reduced from 51 to 5.2 mm, and the M-factor was 40. The greater dispersion allowed a greater reduction in longitudinal emittance at the expense of less transverse cooling. The overall merit factor is not as good as the standard ring.

### B. 66 m circumference ring

A larger circumference ring would allow a longer bunch length of the initial beam and would reduce problems with the injection kicker. The average vertical bending field was 0.064 T. The transmission of an ideal ring after 15 turns was 49%, the transverse normalized emittance was reduced from 11.9 to 2.0 mm, the longitudinal normalized

emittance was reduced from 19 to 6.1 mm, the M-factor was 60, and the D-factor was 5.2. The smaller dispersion hurt the amount of longitudinal cooling and lowered the achievable merit factors.

### **C. 10 MHz ring**

One solution to the problem of a long incoming bunch (train) is to reduce the rf frequency to 10 MHz. Simulations of the 33 m ring were done using a gradient of 2 MV/m and 51° wedges. The transverse normalized emittance of an ideal ring was reduced from 18.6 to 2.9 mm, the longitudinal emittance was reduced from 251 to 79 mm and the M-factor was 61. The transverse cooling was good, but the longitudinal cooling needs more dispersion. The lower gradient was responsible for the slower cooling.

### **D. Open RF cavities**

It is also possible to use open rf cavities in the ring. This eliminates the scattering in the rf windows, but requires more rf power to achieve the same gradient. Simulations with 200 MHz open cavities in an ideal ring obtained the same performance as closed cavities with 50 micron thick windows.

### **E. Cylindrical absorber**

We studied the effect of replacing the “house” shaped absorber with a more practical cylindrical shape. Simulations for an ideal ring using a cylindrical analog to the 100° wedge gave an M-factor of 109 compared to 152 for the house shape.

## **VIII. CONCLUSIONS**

Cooling large emittance muon beams is important for neutrino factories and absolutely essential for a muon collider. Using a ring cooler geometry offers likely economic advantages in reusing expensive magnets, rf cavities and liquid hydrogen absorbers. A ring also provides a natural mechanism for obtaining longitudinal cooling through emittance exchange. The RFOFO ring cooler described here is at this time the most advanced ring cooler design. It uses realistic field modeling and takes into account the effects of windows on the absorbers and rf cavities and the effects of empty cells for injection and extraction. The ring can increase the muon density in a standard acceptance volume by over a factor of 4. However, before such a ring could actually be built, a number of difficult technical issues, such as the injection kicker, need to be resolved through a program of experimental R&D.

## **ACKNOWLEDGMENTS**

This work was supported by the U.S. Department of Energy under contract DE-AC02-98CH10886.

## REFERENCES

1. M. Alsharo'a, *et al*, Recent progress in neutrino factory and muon collider research within the Muon Collaboration, *Phys. Rev. Special Topics-Accelerators and Beams* **6**, 081001-1-52 (2003).
2. C.M. Ankenbrandt, *et al*, Status of muon collider research and development and future plans, *Phys. Rev. Special Topics-Accelerators and Beams* **2**, 081001-1-73 (1999).
3. R.B. Palmer, Ring coolers, *J. Phys.G* **29**, 1577-1583 (2003).
4. V. Balbekov *et al*, Muon ring cooler for the MUCOOL experiment, Proc. 2001 Particle Accelerator Conference, p. 3867-3869.
5. H. Kirk *et al*, Muon storage rings for 6D phase space cooling, Proc. 2003 Particle Accelerator Conference, p. 2008-2010.
6. J.S. Berg, R.C. Fernow, and R.B. Palmer, An alternating solenoid focused ionization cooling ring, MUC-NOTE-COOL-THEORY-239, Mar. 2002. This series of technical notes can be found at <http://www-mucool.fnal.gov/mcnotes/>.
7. J.S. Berg, R.C. Fernow, and R.B. Palmer, RFOFO ring cooler, *J. Phys.G* **29**, 1657-1659 (2003).
8. R.C. Fernow *et al*, Muon cooling in the RFOFO ring cooler, Proc. 2003 Particle Accelerator Conference, p. 2002-2004.
9. J.S. Berg *et al*, RFOFO cooling ring: simulation results, in A. Para (ed), Neutrino Factories and Superbeams, Proc. NuFact03, AIP Conf. Proc. 721, p. 391-4.
10. A. Klier & G.G. Hanson, Simulating the RFOFO cooling ring with GEANT, MUC-NOTE-COOL-THEORY-298, Oct. 2004.
11. V. Balbekov, Investigation of RFOFO-like cooling rings, MUC-NOTE-COOL-THEORY-263, Nov. 2002.
12. V. Balbekov, Simulation of RFOFO ring cooler with tilted solenoids, MUC-NOTE-COOL-THEORY-264, Nov. 2002.
13. R.C. Fernow, ICOOL: a simulation code for ionization cooling of muon beams, Proc. 1999 Particle Accelerator Conference, p. 3020-3022.
14. GEANT – Detector Simulation and Simulation Tool, CERN Program Library Long Write-up W5013, March 1994.
15. R. Raja, MUC\_GEANT – Data Driven GEANT for Ring Coolers, July 2002.  
[http://www.fnal.gov/projects/muon\\_collider/eexchange/Muc\\_GEANT/muc\\_GEANT\\_doc.htm](http://www.fnal.gov/projects/muon_collider/eexchange/Muc_GEANT/muc_GEANT_doc.htm)
16. R.C. Fernow, and J.C. Gallardo, Realistic on-axis fields for the RFOFO cooling ring, MUC-NOTE-COOL-THEORY-265, Nov. 2002.
17. S. Bracker, Magnetic field maps for the RFOFO muon cooling ring, MUC-NOTE-COOL-THEORY-271, Mar. 2003.
18. R.C. Fernow, and J.C. Gallardo, Calculation of RFOFO fields using the off-axis expansion in ICOOL, MUC-NOTE-COOL-THEORY-268, Jan. 2003.
19. R.C. Fernow, J.S. Berg, J.C. Gallardo, and R.B. Palmer, Muon cooling in the RFOFO ring, MUC-NOTE-COOL-THEORY-273, Apr. 2003.
20. S. Ozaki, R. Palmer, M. Zisman & J. Gallardo (eds), Feasibility Study II of a Muon Based Neutrino Source, BNL report 52623, June 2001.
21. ECALC9 was written by G. Penn. For a description of the code see R. Fernow, Physics analysis performed by ECALC9, MUC-NOTE-COOL-THEORY-280, Sep. 2003.
22. R.B. Palmer, L. Reginato & D. Summers, An induction kicker for muon cooling rings, MUC-NOTE-COOL-THEORY-256, Sep. 2002.
23. R.B. Palmer, Cooling efficiency factor, MUC-NOTE-COOL-THEORY-250, Jul. 2002.
24. E. Keil, Muon cooling channels, MUC-NOTE-COOL-THEORY-257, Nov. 2002.